# Multi-Zone Fiber-Optic Intrusion Detection System With Active Unbalanced Michelson Interferometer Used for Security of Each Defended Zone

Hsin Hsieh, Kai-Shuo Hsu, Tai-Lang Jong, and Likarn Wang

***Abstract*—A new fiber-optic system with an active unbalanced Michelson interferometer (AUMI) was designed for multi-zone perimeter intrusion detection by employing only two single-mode fibers for each sensing zone. A pump laser at the monitor site was used to remotely pump the erbium-doped fibers located, respectively, at the two arms of the AUMI for each sensing zone. Configured into a fiber laser cavity, the AUMI served as an optical switch that would modulate the optical power when one arm of the AUMI was perturbed by intrusion to induce a phase offset variation. In the study, an armored cable with a length of 200 meters in total was divided into four sections each guarding a perimeter zone. The experimental results showed that the AUMI system correctly responded to perturbations induced by footstepping on a fiber cable buried underground, vibrating a netted fence, or knocking a window. A high alarm-upon-intrusion rate and zero false alarm rate could be reached by using the presented detection algorithm.**

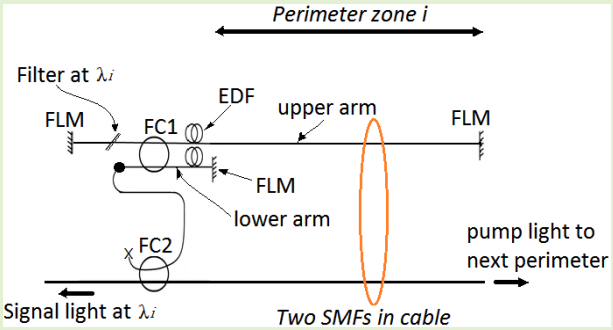


***Index Terms*—Pump laser, Michelson interferometer, multi-zone perimeter intrusion detection, fiber laser cavity.**

## I. Introduction

FIBER-OPTIC perimeter intrusion detection (PID) systems offer some advantages over counterparts using wired or wireless hardwares [1]–[3]. They can find applications in detecting and locating unauthorized excavation of buried pipelines and trespassing intruders in order to protect premises for personal, commercial, and utility purposes.

Many types of fiber-optic PID systems have been recently studied for not only detecting intrusion but providing locating ability for multiple events [4]–[6]. Some of these systems are based on the technique of optical time domain reflectometry (OTDR) and may apply to long-perimeter fields for detection and location of intrusion events. These OTDR-based PID systems in some cases (like in the cases of [4], [6], [7]) require highly coherent lasers in addition to pump lasers, and pulse generators (which involve optical modulators and pulse signal generators). Distributed vibration can be also determined by using optical frequency domain reflectometry with a wavelength-sweeping laser used [8]. A fiber Bragg grating (FBG) secured fence was also demonstrated with an armored-cable packaged FBG array [9]. On the other hand, a full length of perimeter zone can be divided into multiple zones for intrusion detection without based on OTDR technologies. For implementing such a multi-zone PID system, a fiber cable can be configured into multiple perimeter zones [10]–[13] and intrusions can be determined independently at each perimeter zone. And thus simultaneous detection and location of intruders over the total perimeter length is realizable. Using an efficient detection algorithm for eliminating nuisance signals and correctly responding to a true intrusion is a focal point in this type of study [14], [15].

Another issue regarding theimplementation of a multi-zone PID system is the number of single-mode fibers used for detection. As was mentioned in our previous work [16], a multi-zone PID system that uses independent optical circuits

Manuscript received September 4, 2019; accepted October 6, 2019. Date of publication October 11, 2019; date of current version January 17, 2020. This work was supported by the Ministry of Science and Technology, Republic of China, under Grant 107-2221-E-007-051. The associate editor coordinating the review of this article and approving it for publication was Dr. Ioannis Raptis. *(Corresponding author: Likarn Wang.)*

H. Hsieh was with the Institute of Photonics Technologies, National Tsing Hua University, Hsinchu 30013, Taiwan. He is now with Vanguard International Semiconductor Corporation, Hsinchu 300, Taiwan.

K.-S. Hsu was with the Department of Electrical Engineering, National Tsing Hua University, Hsinchu 30013, Taiwan. He is now with Sunplus Technology Co., Ltd., Hsinchu 308, Taiwan.

T.-L. Jong is with the Department of Electrical Engineering, National Tsing Hua University, Hsinchu 30013, Taiwan.

L. Wang is with the Institute of Photonics Technologies, National Tsing Hua University, Hsinchu 30013, Taiwan (e-mail: lkwang@ee.nthu.edu.tw).

Digital Object Identifier 10.1109/JSEN.2019.2946904

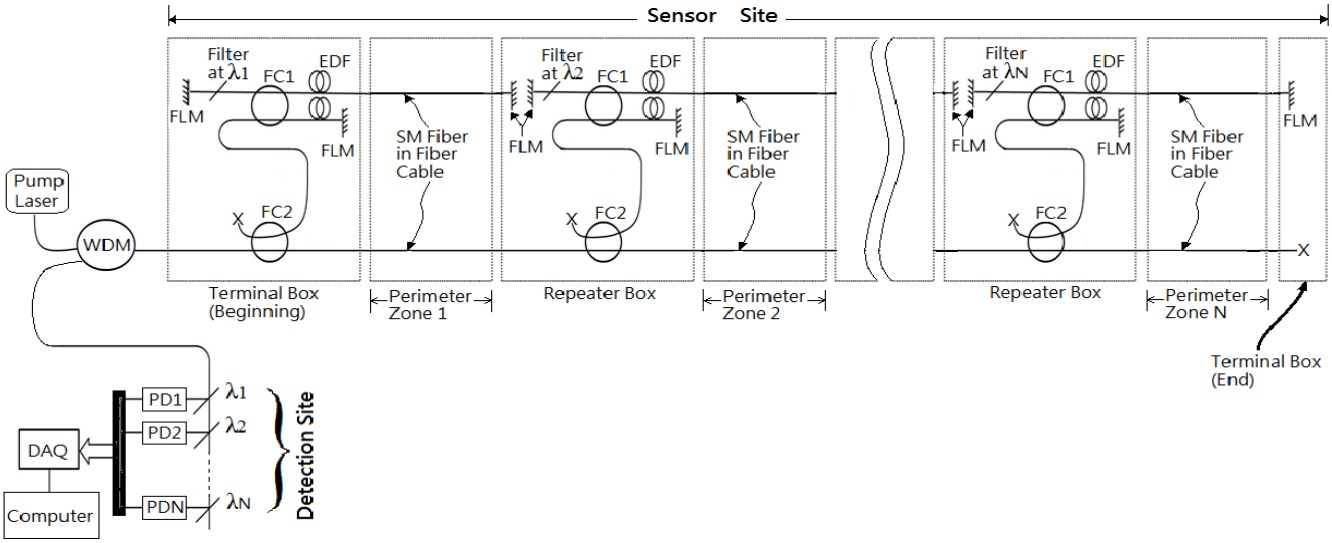


Fig. 1. Proposed PID system configuration for N defended zones. WDM: WDM coupler, Filter: bandpass filter, FC1: 3 dB fiber coupler, FC2: fiber coupler with 10:90 splitting ratio, FLM: fiber loop mirror, EDF: erbium-doped fiber, PD1∼PDN: photodetectors; the symbol x represents bending to nullify reflection at a fiber end. Note that the figure is drawn not to scale.

for each perimeter zone would require a fiber cable containing a bunch of single mode fibers (i.e., a bunch of cores). For example, for the case of N (N = 8, 16 or even 32) perimeter zones with a Michelson interferometer used in each perimeter zone, 2N (i.e, 16, 32 or 64) cores would be needed for the first perimeter zone with the number of cores reduced by two for each subsequent perimeter zone. Although a technique of WDM multiplexing was employed in [17] for a PID system with claimed least number of fiber cores used, that system still required a large number of fiber cores in the fiber cable used, e.g., 5 (7, 9, 11,13,…, 2N+3) cores for the first (second, third, fourth, fifth, …, Nth) perimeter zone.

Here, we propose a new configuration of multi-zone PID system with only two cores used for each perimeter zone. Each perimeter zone contains a local fiber laser cavity (FLC) with a Michelson interferometer as an intrusion detecting sensor as well as an end mirror of the FLC. Two sections of erbium-doped fiber (EDF) are, respectively, spliced into the two arms of the Michelson interferometer, and remotely pumped by a common pump source situated at the monitoring site. The two arms of the Michelson interferometer are different in length, one of which includes the EDF and the pigtails of the components used, while the other further includes the single-mode fiber with the length of the perimeter zone of concern. That is, one core of the fiber cable deployed for detection of the entire perimeter zone is actually one arm of the Michelson interferometer. Another core of the fiber cable is used for pump power delivery and for the transmission of optical detected signal between the sensor site and the detection site. Such a new system is technically different from that of our previous work [16] in that not only are two cores of single-mode fibers used but there would absolutely incur no cross-perimeter interference, unlike in the previous work although the interference is small there.

We have implemented a four-zone PID system, and have observed vibration-induced fluctuations of the detected signals. From such fluctuations we first determined thresholds for real intrusion. Once these thresholds were set, we then tested the proposed PID system upon simulated intrusion. Section two outlines the proposed PID system, explains the principle of operation of the optical system, and then shows the algorithm for determining a real intrusion. Experimental results are presented in section three. There, thresholds for a real intrusion are determined and tested. Section four concludes this paper.

## II. Proposed PID System

### A. Description of the System

Figure 1 shows the PID system for security of N perimeter zones. The sensor site contains N active unbalanced Michelson interferometers (AUMIs) for N perimeter zones, respectively. Each AUMI comprises a 3 dB fiber coupler (FC1) and unbalanced fiber arms that are each ended with a fiber loop mirror (FLM) formed by connecting the two ports of a 3 dB fiber coupler at one side. Two sections of EDF are, respectively, spliced into the two fiber arms, providing optical gains for beam propagation within the FLC when pumped by a pump power delivered from a pump laser at the monitor site. Each AUMI is a part of the corresponding FLC, and serves as an optical switch for modulating the lasing light. The FLC is composed of an AUMI, an FLM, and a bandpass filter which defines the lasing wavelength at $\lambda$i (i = 1,2,…,or N).

A 1480 nm pump laser is used for remotely pumping all the EDFs in the AUMIs. First, the pump light, after passing through a wavelength division multiplexing (WDM) coupler, delivers its power to the two EDFs through a 10:90 fiber coupler (FC2) and then FC1 in the beginning terminal box. In this terminal box, 10% of the pump power is directed to FC1, and the other 90% proceeds down a single-mode (SM) fiber in the fiber cable that is used for security of perimeter zone 1 to the adjacent repeater box, where again 10% of the pump power is tapped by FC2 there and used for pumping the two EDFs in the AUMI, whereas the other 90% is directed to the next repeater box through a SM fiber that is used for security of perimeter zone 2. The pump power gradually

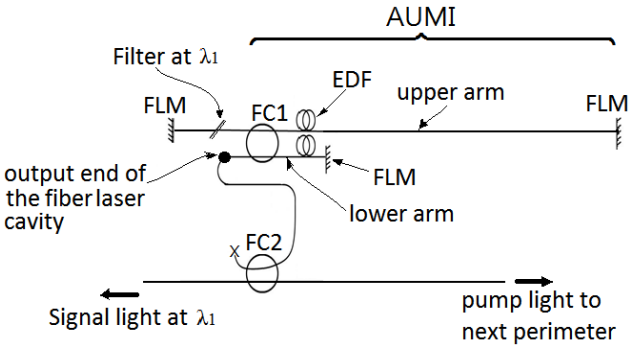


Fig. 2. Fiber laser cavity containing an AUMI for perimeter zone 1.

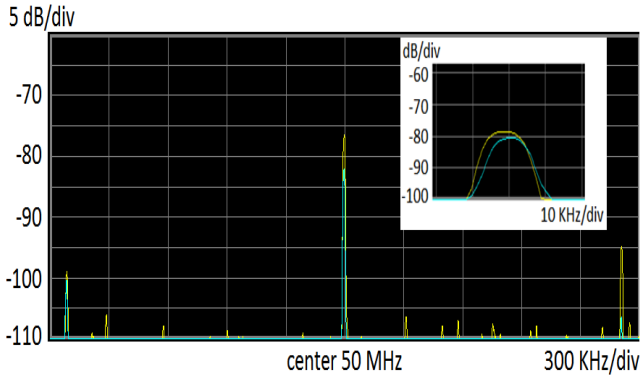


Fig. 3. Spectrum of the lasing light of the FLC measured by using the delayed self-heterodyne method with an AO frequency shifter (50 MHz) incorporated in one arm of the Mach-Zehnder interferometer that has an offset length of 50 km. The inset shows the magnified central peak of the spectrum. The two traces represent instantaneous and average results, respectively.

decays as the pump light proceeds up to the last repeater box. The whole system is terminated by an end terminal box, which contains a section of fiber bent into a coil (denoted by a symbol x) as well as an FLM that reflects the light in an fiber arm of the AUMI for perimeter zone N. Unused fiber ends are likewise bent into coils to avoid end reflection at other places denoted by the symbol x. It is noticeable that in each perimeter zone, only two SM fibers are used for sensing the vibration or perturbation on the fiber cable caused by intruders. Notably, one of the SM fibers in each perimeter zone serves as an arm of the AUMI, i.e., the sensing arm, whereas the other is used only for optical power delivery of the pump light and the signal light between the sensor site and the detection site. Here, the sensor site includes terminal boxes, repeater boxes and perimeter-zone fiber cables, whereas the detection site mainly contains WDM thin film filters at $\lambda$i (i = 1,2,…, and N), photodetectors (PDi, i = 1,2,…, and N), a data acquisition (DAQ) module, and a computer. When there is no perturbation on this SM fiber arm of the AUMI, a constant lasing light at a wavelength defined by the bandpass filter is emitted at an end of FC1 and propagates down to the WDM coupler through FC2, and reaches the corresponding photodetector at the detection site. The WDM thin film filters are cascaded to de-multiplex the lasing lights from different FLCs. Optical power variations of the lasing lights detected at the detection site are then acquired by the DAQ module and analyzed by a software algorithm to determine if there is an intrusion at a perimeter zone.

### B. Operational Principle of AUMI

We use the AUMI of perimeter zone 1 (Fig. 2) to explain how the AUMI operates and gives rise to a fluctuation in the optical power of the lasing light emitted at the output end of the fiber laser cavity as the upper arm of the AUMI is perturbed. As mentioned previously, the fiber laser cavity for each perimeter zone is composed of an FLM at one end (i.e., the FLM on the left hand side in Fig.2) and an AUMI at the other end, the latter of which serves as a variable reflector. As shown in Fig.2, the AUMI has a longer arm (i.e., the upper arm), which is one SM fiber of the fiber cable and may be tens of meters or more than a hundred meters in length practically, and a shorter arm (i.e., the lower arm), which is several meters long. An optical gain is provided by the pumped EDF spliced into each arm. The wavelength of the lasing light in the laser cavity is defined by a bandpass filter. The spectral width of the lasing light of the FLC in the case was measured to be about 5 kHz by using the delayed self-heterodyne method with an AO frequency shifter (shifting the frequency by 50 MHz) in a fiber arm of the Mach-Zehnder interferometer that has an offset length of 50 km. The laser spectrum measured by using an electric spectrum analyzer (Model N9030A, Agilent Technologies) is shown in Fig. 3. The difference between the powers of the main peak and the strongest side peak is at least 32 dB, indicating a single mode characteristics.

When the upper arm is perturbed, the AUMI back-reflects a light with its power fluctuating with the variation of the phase offset $\delta$ between the two arms. The output light of the AUMI is dependent on $1 - \tau \cos \delta$, where $\tau$ is related to the polarization effect [18]. When an intruder perturbs the fiber arm, the output light intensity varies accordingly, and the power of the lasing light of the FLC changes dynamically (i.e., generates an oscillating light) as well. The oscillating light produces a fluctuating signal light (laser light) at the output end of the fiber laser cavity. Then the output signal light propagates through the fiber coupler FC2 and the WDM coupler, and is finally detected by the corresponding photodetector at the detection site.

The fiber cable for perimeter zone 1 was placed on a grassland, but most parts of it were suspended by weeds in the experiment conducted here. Figure 4 shows the signal waveforms detected by the photodetector when the AUMI was perturbed as the fiber cable was vibrated slightly by a 6 m/sec wind (top trace), struck by a tennis ball of 55 gw (gram weight) falling from a height of 16 cm (middle trace), and struck by a steel ball of 350 gw (bottom trace) falling from the same height.

### C. Algorithm for Determining Intrusion

In this study, signal waveforms for the cases of nonintrusion and intrusion were detected and collected in a simulative field test to establish a data base, and then the data were analyzed in both time and frequency domains. Two thresholds for alarming an intrusion were determined. One of the thresholds for alarm

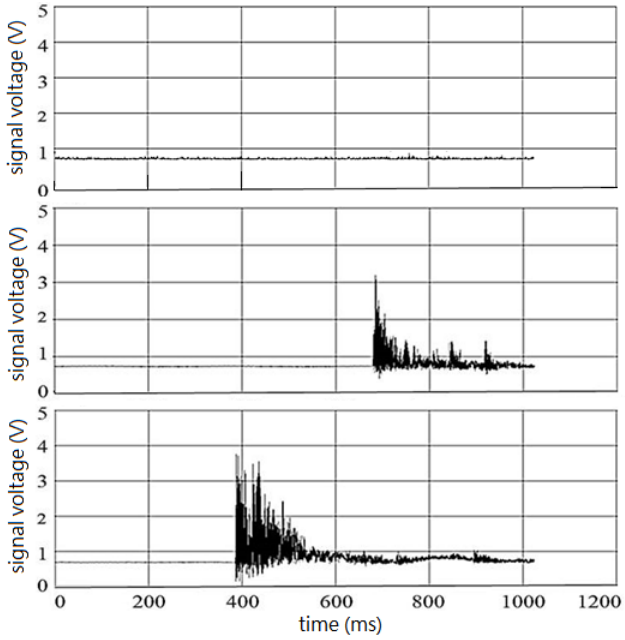


Fig. 4. Signal waveforms detected by the photodetector for perimeter zone 1 when the corresponding AUMI is perturbed as the fiber cable containing the AUMI was placed on a grassland and was vibrated slightly by a 6 m/sec wind (top trace), struck by a tennis ball of 55 gw (middle trace), and struck by a steel ball of 350 gw (bottom trace).

is the threshold for the normalized voltage amplitude (NVA) that is defined by

$$\text{NVA} = (V_{max} - V_{min})/V_{avg} \tag{1}$$

where $V_{max}$ ($V_{min}$) is the maximum (minimum) voltage of the detected waveform, and $V_{avg}$ is the average voltage of the detected waveform over a time period of data acquisition, which is 1.024 sec in the study. From the case of Fig.4, we can see that NVA is large when the AUMI is well perturbed (or the perimeter zone is maliciously intruded) in contrast to the negligibly small NVA for the nonintrusion case exemplified by the top trace. The intrusion-induced fluctuation in optical power of the signal light corresponds to an NVA that is above some critical level or a threshold. Below the threshold, any perturbation upon AUMI, even causing some fluctuation in optical power of the signal light, is not considered as an event of intrusion. However, there is a gray area in judging if an event is a case of intrusion or nonintrusion by checking the amplitude of the signal fluctuation solely. For example, when a bird flies down to the fiber cable and vibrates it, when a dog scratches the net to vibrate the fiber cable, or when heavy rain/ hailstones beat against the net to vibrate the fiber cable, the amplitude of the signal fluctuation may be large momentarily and therefore the NVA may sometimes exceed the threshold that was set beforehand. In this case, a false alarm could be triggered. To avoid this problem, signals in the frequency domain need to be processed.

We note that the signals caused by nuisance can be discriminated from those caused by an event of intrusion in the frequency domain. Nuisance signals caused by small animals and environmental factors such as wind or rainfall

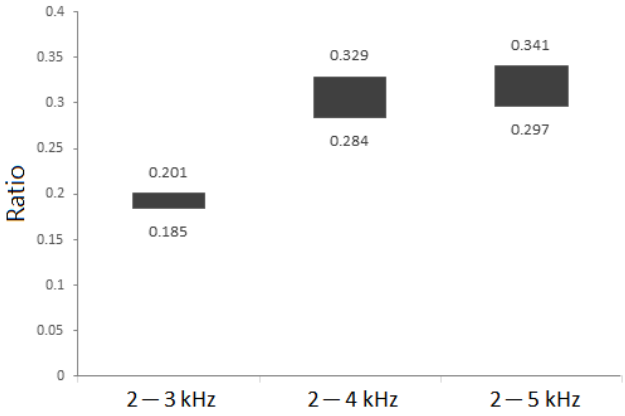


Fig. 5. The ratios of the integrated spectral strength over the bands of 2–3 kHz, 2–4 kHz, and 2–5 kHz to that over the whole frequency band for the case in which a baseball of 158 gw falling from a height of 16 cm struck the fiber cable of perimeter zone 1.

might exhibit weaker amplitudes at high signal frequency components than the intrusion signals. If this is the case, intrusion signals can be discriminated from nuisances. Thus, in this study, we took the fast Fourier transform of the real-time signal waveform detected to acquire the weighting factor of the spectral components in a specific range of higher frequencies. This weighting factor is defined as the ratio (denoted by Ratio hereafter) of the integrated spectral strength over a concerned frequency range to that over the whole frequency band (excluding the DC). Since a low-pass filter was used to filter spectral components of noises higher than 5 kHz, the band up to 5 kHz was considered as the whole frequency band here. When the fiber cable of perimeter zone 1 was struck by a baseball of 158 gw falling from a height of 16 cm, the ratios of the integrated spectral strength over the bands of 2 – 3 kHz, 2 – 4 kHz, and 2 – 5 kHz to that over the whole frequency band (excluding the DC component) are shown in Fig.5. The upper and lower bounds of each range are indicated by the numbers shown aside. The spectral content of the signal waveform upon strike was obtained by fast Fourier transform, and then the ratios for the three bands were calculated. The strike was repeated 60 times, resulting in a range of the ratio for each band as shown in the figure. It can be seen that most spectral power resided in a range no larger than 2 kHz. Since nuisance signals usually have stronger low-frequency strengths than intrusion signals, we would give an emphasis on high-frequency components that discriminate intrusion signals from nuisances. In this study, we chose the band of 2 – 4 kHz for determining the ratio.

## III. Experiments and Results

### A. Deployment of Fiber Cable

In the study, two cores (i.e., two single-mode fibers) of a 4-core armored cable was employed to realize a simulative four perimeter-zone intrusion detection system. The layout of the fiber cable is shown in Fig. 6, where the fiber cable of totally 200 m in length was sectioned into 4 perimeter zones with 50 m for each.

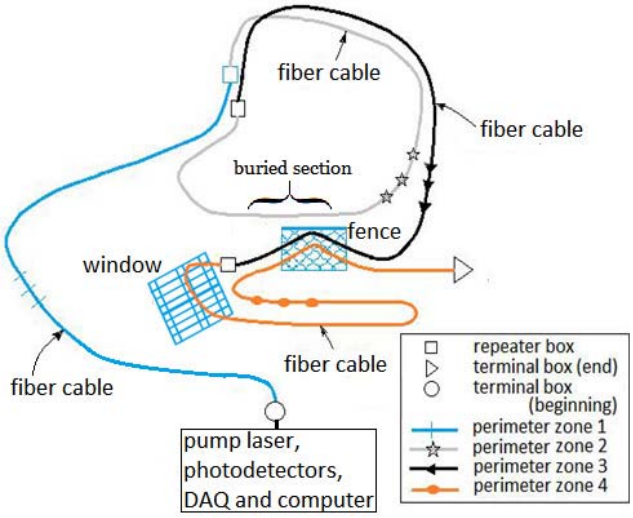


Fig. 6. Layout of simulative four-perimeter-zone intrusion detection system in the study.

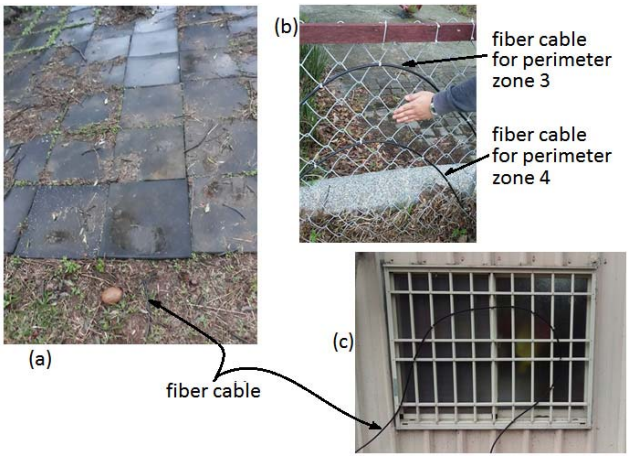


Fig. 7. Fiber cables (a) buried underground and then covered by rubber tiles, (b) attached on a soft netted fence, and (c) fixed on a grille.

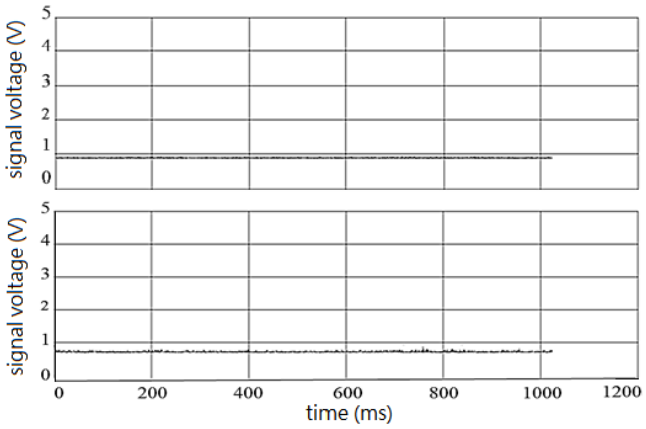


Fig. 8. Signal waveforms detected by the photodetector for perimeter zone 1 when the corresponding fiber cable was unperturbed (upper trace) and was perturbed by a wind of 6 m/sec in speed (lower trace).

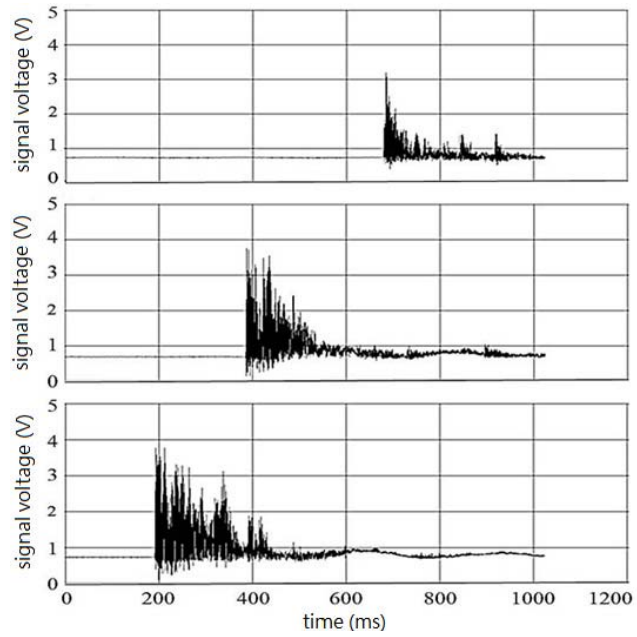


Fig. 9. Signal waveforms detected by the photodetector for perimeter zone 1 when the corresponding fiber cable was struck slightly (top trace), moderately (middle trace), and heavily (bottom trace).

The fiber cables for the whole perimeter zones lay on a grassland except for a small part. For example, an ∼2 m long fiber cable at the starting part of perimeter zone 1 hung down to the grassland from the beginning terminal box that was placed on a worktable, whereas a section of fiber cable also in the length of ∼2 m at perimeter zone 2 was buried underground in depth of about 13 cm and then covered by rubber tiles (see Fig. 7(a)). Besides, both perimeter zones 3 and 4 had a short length (about 1.2 meter) of fiber cable attached on the same fence so that we could simulate simultaneous intrusions at the two perimeter zones (see Fig. 7(b)). We also fixed a short length of perimeter-zone-4 fiber cable on the grille of a window to simulate an intrusion on a grille (Fig. 7(c)). These sections of fiber cable for perimeter zones 2, 3 and 4 were tested to determine intrusions, whereas the other parts of the fiber cables for these perimeter zones were not a concern but to generate some sort of nuisances in the test. We were aware that the fiber cable would in fact hang in air even it lay tight on the grassland. The aforementioned hanging part of fiber cable for perimeter zone 1 was susceptible to wind, and so were all other hanging parts of the fiber cables for all the perimeter zones. When the wind came to disturb the AUMIs of these perimeter zones, optical power fluctuation could be observed.

The 1480 nm pump laser delivered a power of 250 mW to the sensor site to pump the EDFs located at the fiber arms of the four AUMIs. Each EDF section had a length of 5 m in the study. The EDF was of the same type used in [16]. The lasing wavelengths (pump powers) for the four perimeter zones were, respectively, 1550.12 nm (23.4 mW), 1557.36 nm (19.9 mW), 1558.98 nm (17.4 mW), and 1560.61 nm (15.6 mW)

## B. Determination of Thresholds

*1) Perimeter Zone 1:* Figure 8 shows the waveforms detected by the photodetector when there wasn't a wind (upper trace)

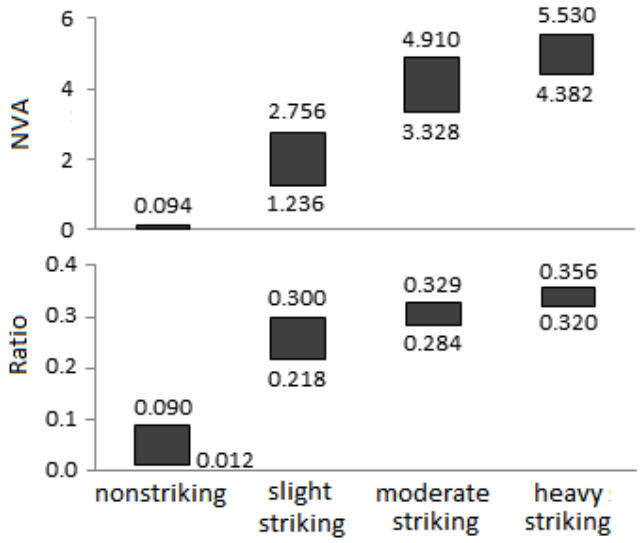


Fig. 10. Ranges of NVA and Ratio obtained for perimeter zone 1 when the fiber cable was unstruck, slightly struck, moderately struck, and heavily struck by external forces.

and there was a wind in the speed of 6 m/sec (lower trace). Quite clearly, the wind only perturbed slightly the AUMI, inducing an unremarkable fluctuation in the waveform.

Although the fiber deployment for perimeter zone 1 could not represent the practical case for testing the intrusion detection, we would still demonstrate the perceptibility of the AUMI to the vibration incurred on the fiber cable. Three balls having weights of 55 grams, 158 grams and 350 grams, respectively, fell from a height of 16 cm and then struck the fiber cable that lay on the grassland. The three balls exerted a force and perturbed the AUMI slightly, moderately and heavily, respectively. The detected waveforms for the strike cases are shown in Fig. 9, where one can see that the moderate and heavy strikes produced not too far different signal amplitudes, whereas the slight strike generated a smaller signal amplitude.

The fiber cable was slightly struck, moderately struck, and heavily struck 60 times for each case. Then the ranges of NVA and Ratio for these three cases were calculated and compared with those ranges calculated from the signal waveforms obtained for a time period of 90 seconds when the fiber cable was unstruck. Figure 10 shows the comparison. We can see that there is a clear difference between the cases of nonstriking and striking for both NVA and Ratio.

*2) Perimeter Zone 2:* We first check the detected signal when a man steps on top of the fiber cable (stepping position 1) and 50 cm away from the fiber cable (stepping position 2), as shown in Fig.11.

Figure 12 shows the detected signal waveforms when no one stepped on the rubber tiles (top trace), when a man repeatedly stepped on the rubber tile at stepping position 2 (middle trace), and when that man repeatedly stepped on the rubber tile right at stepping position 1 (bottom trace). It should be noted that the test was performed on a sunny day with a breeze, and that the signal oscillation would become even larger than the bottom trace of this figure when a man walked away from stepping position 1 at his last footstep (not shown here).

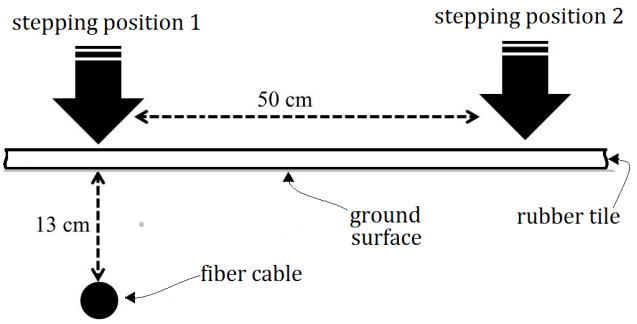


Fig. 11. A part of the fiber cable for perimeter zone 2 was buried underground.

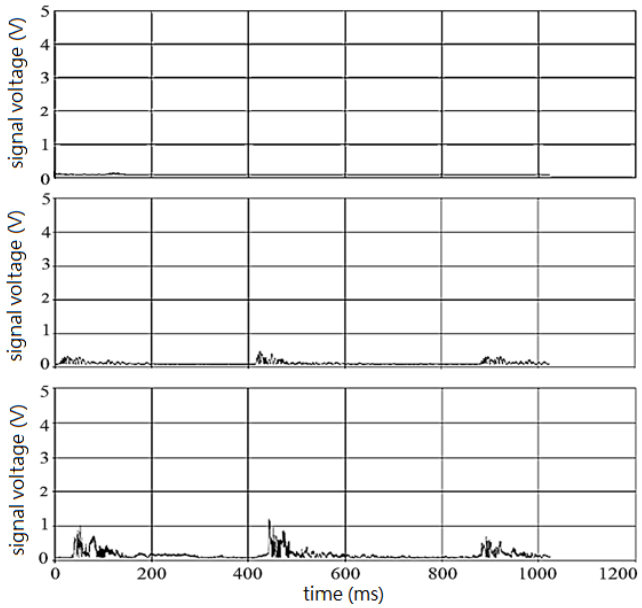


Fig. 12. Signal waveforms detected by the photodetector for perimeter zone 2. Top trace: when no one stepped on the rubber tiles where a section of fiber cable was buried underneath. Middle trace: when a man repeatedly stepped on the rubber tile at a position 50 cm away from the buried fiber cable. Bottom trace: when a man repeatedly stepped on the rubber tile right on top of the buried fiber cable.

Figure 13 shows the detected signal waveforms when a man walked toward the rubber tiles. The traces from top to bottom corresponded to the man's positions of 100 cm, ~60 cm, ~30 cm and 0 cm away from the buried fiber cable, respectively. Last footstep on right top of the buried fiber cable resulted in a strong signal magnitude as indicated by the left signature in the bottom trace, whereas a next footstep that was ~30 cm away from the buried fiber cable produced a weaker signature. It is noted here that we may set the limit for the secured distance as we wish it to be, and that an intrusion alarm should be triggered once anyone passes by the area within this limit. In this study, we set a distance of 50 cm for the limit.

We then calculated the values of NVA and Ratio from the signal waveforms obtained by having a man step repeatedly on the rubber tiles at a position 50 cm away from the fiber cable as well as at right top of the fiber, respectively. Sixty consecutive signal waveforms were then used for each case

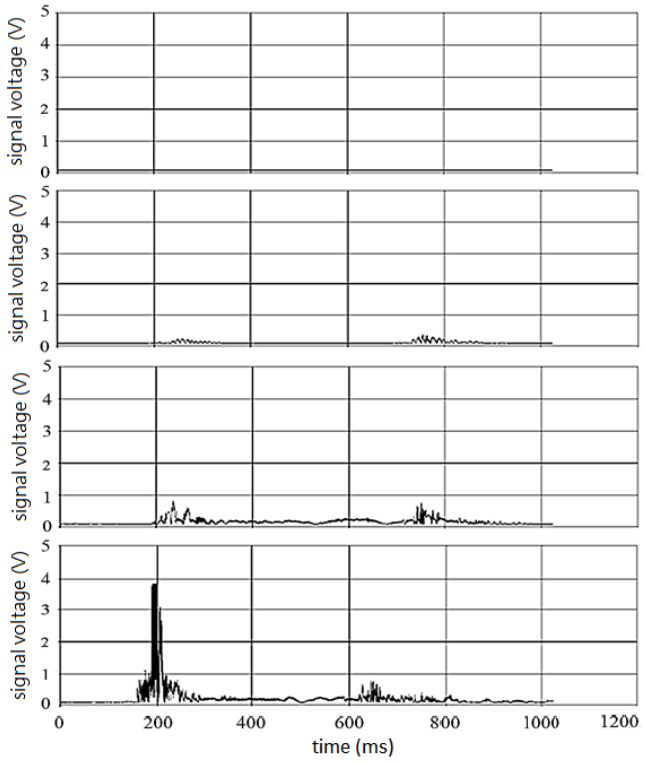


Fig. 13. Signal waveforms detected by the photodetector for perimeter zone 2 when a man walked toward the rubber tiles where a section of fiber cable was buried underneath. The traces from top to bottom corresponded to the man's positions of 100 cm, ~60 cm, ~30 cm and 0 cm away from the buried fiber cable, respectively.

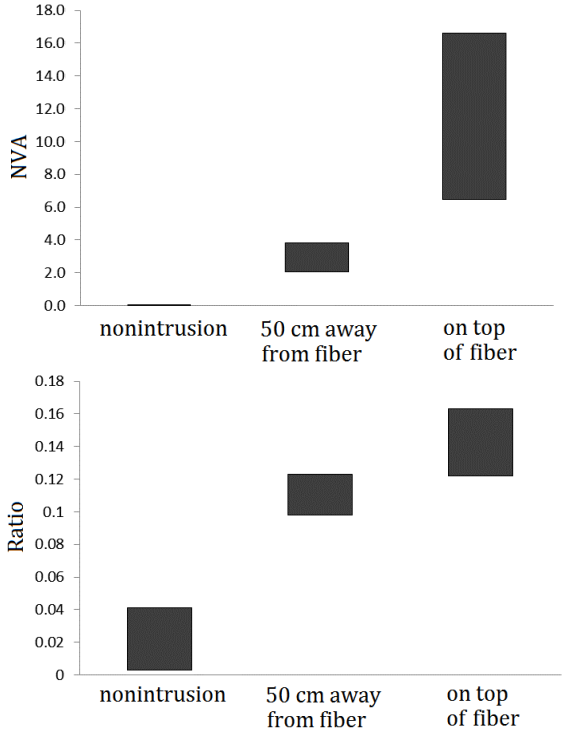


Fig. 14. Ranges of NVA and Ratio obtained for nonintrusion case and for the case when a person repeatedly stepped on the rubber tiles at a position 50 cm away from the fiber cable as well as at right top of the fiber cable.

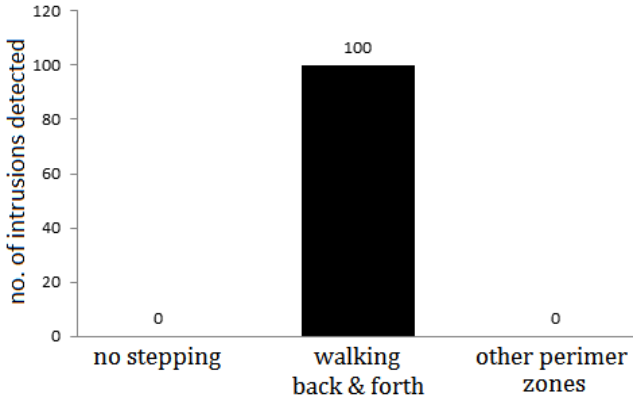


Fig. 15. Number of intrusions detected for perimeter zone 2 for the case of no stepping, and for the case in which a man walked back and forth for 50 times on the rubber tiles within 1 meter. The numbers of intrusions detected by other perimeter zone detectors were all zero.

of position. The results are shown in Fig.14, where NVA and Ratio for the case of nonintrusion are also shown for comparison. We found that both NVA and Ratio fell into a range for each case, and that either NVA or Ratio for both cases of stepping positions distributed differently. When the man stepped right on top of the fiber cable, NVA went larger and distributed in a wider range compared with the case in which he stepped at a position 50 cm away. Stepping at right top of the fiber cable also made a larger Ratio in contrast to the case of stepping 50 cm away from the fiber cable. In the nonintrusion case, data were recorded consecutively for more than 90 seconds and then analyzed to give NVA and Ratio as well. It was found that these values of NVA and Ratio were comparatively small with respect to the stepping cases. Therefore, we could tell whether there was a man stepping near the fiber cable by checking in a real time manner if both NVA and Ratio exceeded preset values (i.e., thresholds), respectively. In the study, the threshold for NVA could be set to be 1.9, which was a little bit smaller than the lower limit of the range, 2.05, for the case of stepping at a position 50 cm away from the fiber cable and far above the upper limit of the range, 0.055, for the nonintrusion case. The reason for the asymmetric choice of the threshold that was close to 2.05 and far from 0.055 arose from the fact that small animals running and hailstones falling on the rubber tiles would cause an increase in NVA. On the other hand, the threshold for Ratio was set to be 0.06, which was met by stepping at a position within 50 cm.

Figure 15 shows the number of intrusions detected for perimeter zone 2 for the case of no stepping, and for the case in which a man walked back and forth for 50 times on the rubber tiles within 1 meter from the fiber cable. The figure also shows the number of intrusions detected by other perimeter-zone detectors. As shown in the figure, when there was no stepping occuring (i.e., in the nonintrusion case), no intrusion was detected during a time period of 20 minutes, indicating zero false alarm rate in the study. On the other hand, when a man walked across the security zone (which had a width of 1 meter with the center on the buried fiber

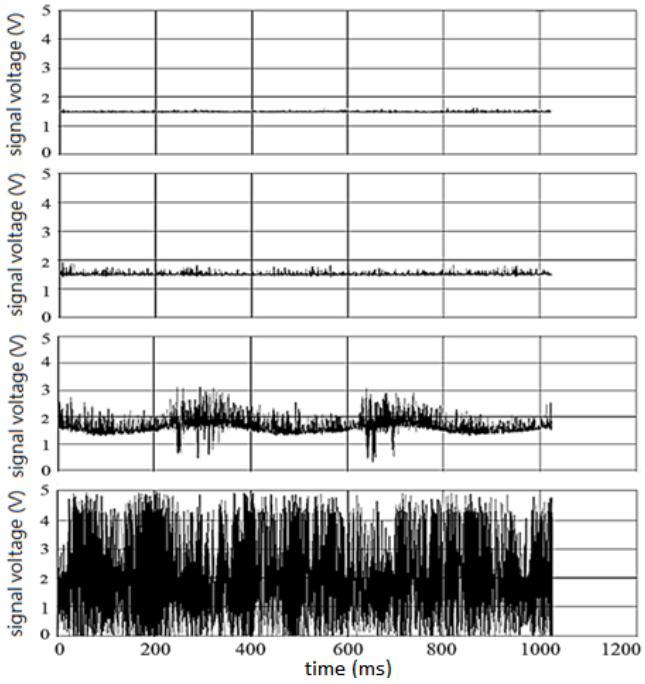


Fig. 16. Signal waveforms detected by the photodetector for perimeter zone 3 when the corresponding AUMI was unperturbed (top trace); when the fiber cable on a netted fence was vibrated slightly by a 6 m/sec wind (the second trace from the top); when the netted fence was manually shaken to result in an oscillation amplitude of 2 cm (the third trace), and an oscillation amplitude of 10 cm (bottom trace).

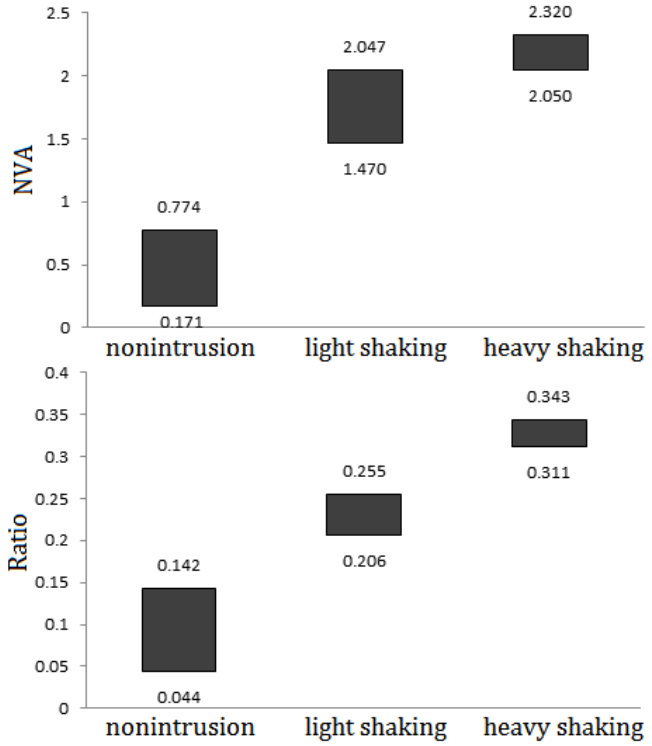


Fig. 17. Ranges of NVA and Ratio obtained for nonintrusion case and for the cases when the netted fence was shaken to result in oscillation amplitudes of 2 cm (light shaking) and 10 cm(heavy shaking).

cable), 100 time intrusions were detected by this perimeter zone detector, demonstating an alarm rate of 100% accuracy. Meanwhile all other perimeter zone detectors did not detect an intrusion, indicating no crosstalk effect. Also, we have observed that the signal waveforms for other perimeter zones did not change upon intrusion at this perimeter zone.

*3) Perimeter Zone 3:* To simulate a nuisance aroused by a small animal, we shook the fence (by knocking) such that the net vibrated with an oscillation amplitude of 2 cm (peak to peak). A real intrusion was simulated by shaking (i.e.,knocking) the net to have an oscillation amplitude of 10 cm (peak to peak). In both cases, 60 times of shakings were made, respectively, and the values of NVA and Ratio were determined therein. For the case of nonintrusion, signal waveforms were consecutively acquired over 90 seconds.

Figure 16 shows the signal waveforms detected by the photodetector for perimeter zone 3 when the corresponding AUMI was unperturbed (top trace) and perturbed (the other three traces). The second trace from the top was obtained when the netted fence was vibrated slightly by a 6 m/sec wind. The third trace and the bottom trace were for the case when the net was manually shaken to result in oscillation amplitudes of 2 and 10 cm, respectively.

Figure 17 shows the ranges of NVA and Ratio for the nonintrusion case and for the cases when the netted fence was shaken to result in oscillation amplitudes of 2 cm (light shaking) and 10 cm (heavy shaking). To detect a real intrusion, a threshold for NVA was set at a value smaller than the lower bound for heavy shaking, which we chose to be 1.9 in the study. We can see that some cases of light shaking would exceed this threshold. However, we can see that there is a gap between the lower bound of Ratio for heavy shaking and the upper bound of Ratio for light shaking, and therefore a threshold value of Ratio can be set at a value somewhere in the gap. In the study, we set the threshold of Ratio at 0.3 to guarantee that lightly shaking the fence would not cause the value of Ratio to exceed the threshold,whereas heavily shaking the fence would break through the threshold. Therefore, the thresholds of NVA and Ratio are to be met at the same time to determine an intrusion, which corresponds to the case of heavy shaking in the study.

*4) Perimeter Zone 4:* As noted for this perimeter, a part of fiber cable was attached on a netted fence and a part of fiber cable was attached on a grille. Because these parts responded differently to the impact by an intruder, they are discussed in separate cases. Figure 18 shows the signal waveforms detected by the photodetector for perimeter zone 4 when the fiber cable of this perimeter zone wasn't perturbed (top trace), when the fiber cable on the fence was vibrated slightly by a 6 m/sec wind (the second trace from the top), when the fence was shaken to result in an oscillation amplitude of 2 cm (the third trace), and when the fence was shaken to result in an oscillation amplitude of 10 cm (bottom trace).

Figure 19 shows the signal waveform detected by the photodetector when a man knocked the grille. We can see that an oscillation occurs every 0.3 second, which corresponds to the man's knocking frequency.

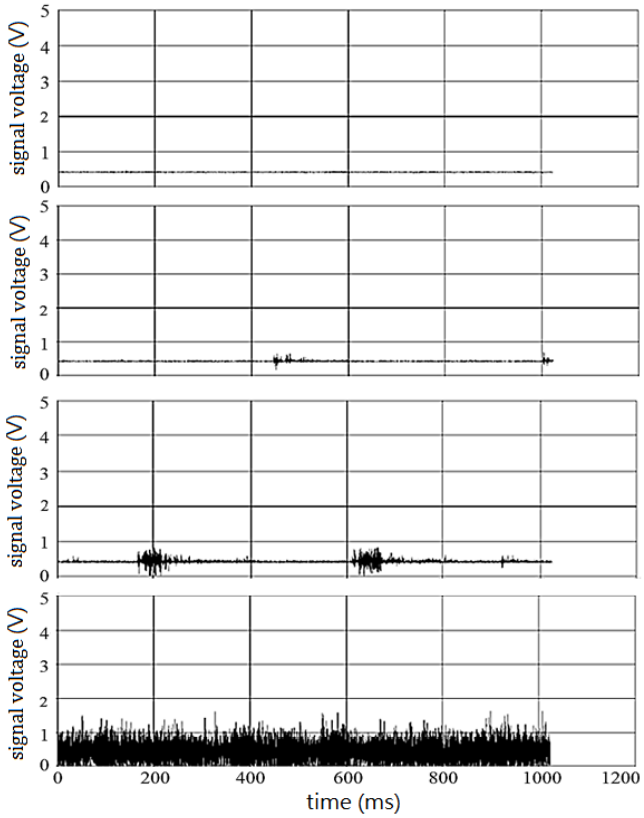


Fig. 18. Signal waveforms detected by the photodetector for perimeter zone 4 when the corresponding AUMI was unperturbed (top trace); when the fiber cable on a netted fence was vibrated slightly by a 6 m/sec wind (the second trace from the top); when the fence was manually shaken to result in oscillation amplitudes of 2 cm (the third trace) and 10 cm (bottom trace).

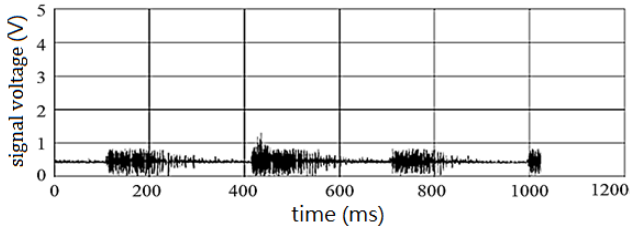


Fig. 19. Signal waveforms detected by the photodetector for perimeter zone 4 when a man knocked the grille.

Figure 20 shows the ranges of NVA and Ratio obtained for perimeter zone 4 when the fiber cable was not perturbed (nonintrusion), when the netted fence was shaken to result in oscillation amplitudes of 2 cm (lightly shaking the fence) and 10 cm(heavily shaking the fence), and when the grille was knocked (grille tapping). The lower and upper bounds of the ranges are indicated by the numbers aside.

In the fence-secured system, we set thresholds of NVA and Ratio at 2.5 and 0.395, respectively, for determining an intrusion, which corresponded to the case when the fence was heavily shaken. When the fence was lightly shaken owing to small animals' touching, both values of NVA and Ratio were expected not to exceed the two thresholds, respectively. Although the value of Ratio might sometimes accidentally

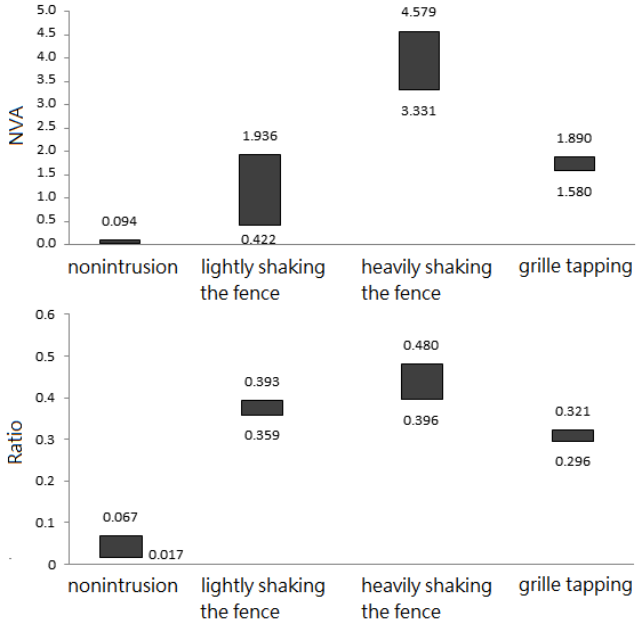


Fig. 20. Ranges of NVA and Ratio obtained for perimeter zone 4 when the fiber cable was not perturbed (nonintrusion), when the netted fence was shaken to result in oscillation amplitudes of 2 cm (lightly shaking the fence) and 10 cm (heavily shaking the fence), and when the grille was knocked (grille tapping). The lower and upper bounds of the ranges are indicated by the numbers aside. The lower bound of NVA for nonintrusion case is close to zero.

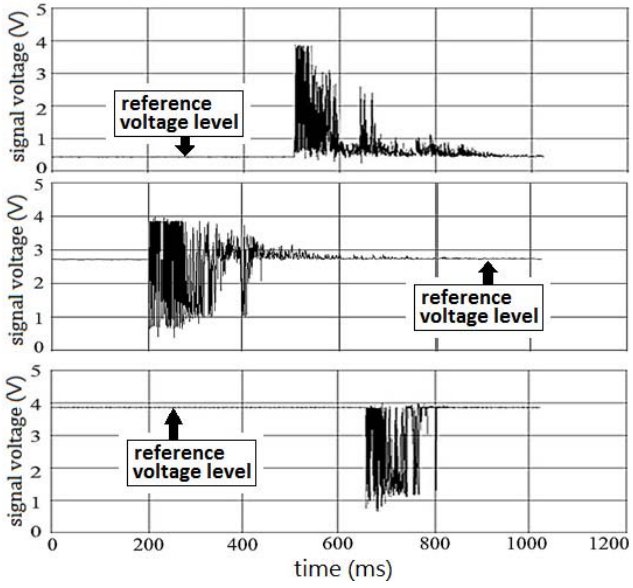


Fig. 21. Signal waveforms detected by the photodetector for perimeter zone 1 when the corresponding fiber cable was struck slightly for reference voltage levels of 0.5 V (top trace), 2.7 V (middle trace), and 3.9 V (bottom trace).

exceed the threshold owing to such touching, values of NVA would not easily exceed the threshold in this case. Only when the fence is heavily shaken to get the two thresholds met at the same time, will an alarm be triggered.

On the other hand, when we consider the case of grille defense, the fiber cable is to be perturbed as the iron bars are knocked or struck. From the ranges of NVA and Ratio shown

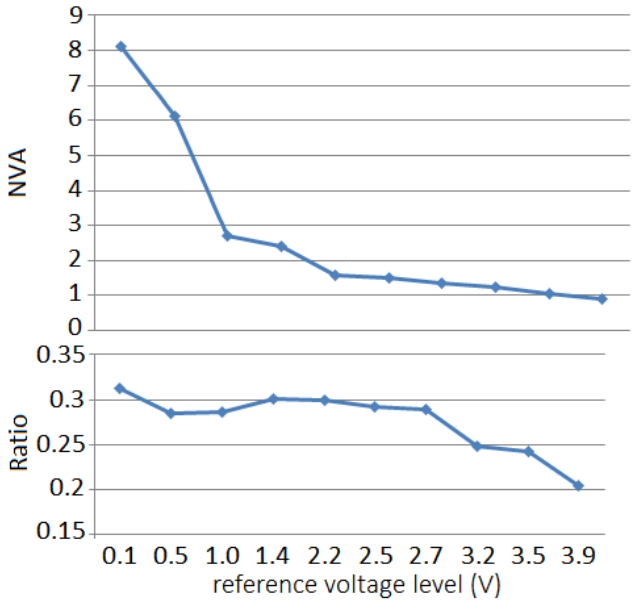


Fig. 22. NVA and Ratio measured for each reference voltage level varying from 0.1 V to 3.9 V.

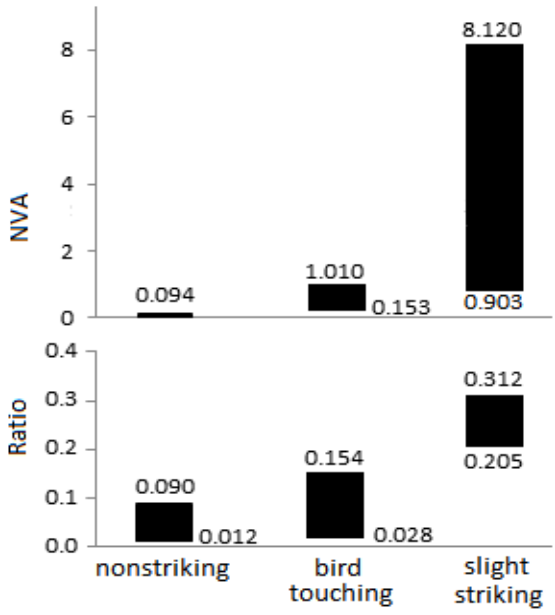


Fig. 23. Range of NVA and Ratio for the cases of nonstriking, bird touching and slight striking.

in Fig. 20, we can see that the lower bounds of the two ranges for knocking the grille (see the case of grille tapping) are well discriminable from the nonintrusion case, and thus one can set the thresholds to be 1.5 (for NVA) and 0.2 (for Ratio).

### C. Testing the PID System

Once the thresholds of NVA and Ratio are set, we are ready to test the performance of the PID system in a simulative study. In the test, we vibrated the fiber cable of each perimeter zone by striking the fiber cable (for perimeter zone 1), walking around the area with a fiber cable buried underground (for perimeter zone 2), shaking the netted fence (for perimeter zones 3 and 4), and knocking the grille on its iron bars (for perimeter zone 4), to see how well or bad the detection algorithm worked. We vibrated the fiber cable 100 times in each case of intrusion, and the total number of intrusions detected were counted. To test the false alarm rate for the case of nonintrusion, the total number of intrusions detected was monitored over a time period of 20 minutes.

The test results are summarized below. For buried fiber cable at perimeter zone 2, walking back and forth for 50 times caused 100 alarms for intrusion, while no intrusion was detected for other perimeter zones. When the fence was heavily vibrated 100 times, the algorithm counted 100-time intrusions for both perimeter zones 3 and 4 because they both had a fiber cable on the same fence. We found no intrusion detected for perimeter zones 1 and 2. Because the NVA and Ratio thresholds were set for heavily shaking the netted fence, the test results for lightly shaking the fence were zero intrusion detected for both perimeter zones 3 and 4. Then we knocked the fiber cable at perimeter zone 3 that was not on the fence to induce 100-time intrusion alarms for perimeter zone 3, in which case no intrusion was detected for perimeter zone 4. The same thing happened for the case when the roles of these two perimeter zones were switched.

Also we preset the NVA and Ratio thresholds for the perimeter zone 1 at the values of 0.9 and 0.18, respectively, which were met by slight striking. Then, we could detected 100-time intrusions no matter when the fiber cable was slightly struck, moderately struck, or heavily struck for 100 times. In these cases, no intrusion was detected for other perimeter zones. It should be emphasized that the detected signal waveforms for a perimeter zone would not be affected at all by perturbation on the fiber cable of any other perimeter zone.

In the test for knocking the grille, we found 100-time intrusions if a man knock the grille on the iron bars 100 times, and meanwhile no intrusion was detected for other perimeter zones. Next, when all fiber cables of the four perimeter zones were neither struck, knocked, shaken, nor been stepped on, no intrusion was detected for all the four perimeter zones.

## IV. Effect of Temperature

Because of the large path length imbalance between the two arms of the Michelson interferometer, the reference voltage level (denoted by RVL, which corresponds to the voltage level when no signal oscillation is induced) may vary with the environmental temperature. We explore this issue by taking perimeter zone 1 for example. Experiments with this perimeter zone were conducted from 11 AM (hot) to 7 PM (cool) in the same day, and the RVL was found to vary in a 3.9 volt range (noting that the output voltage for this photodetector was clamped to ~3.9 V). Figure 21 shows signal waveforms detected when the corresponding fiber cable was struck slightly for RVLs of 0.5 V (top trace), 2.7 V (middle trace), and 3.9 V (bottom trace).

TABLE I
COMPARISON OF VARIOUS TECHNOLOGIES FOR INTRUSION DETECTION

| Technology | Number of fibers used in fiber cable | Length of total protected area | Spatial resolution | Type of light source used |
|---|---|---|---|---|
| $\phi$-OTDR | 1 | 1.2 km[7], 12 km[4], or 131 km [6] | laser pulsewidth dependent | highly coherent laser |
| FBG[9] | 1 | 72 m | 7.2 m | broadband |
| MZ/Sagnac[5] | 1 | 41 km | < 200 m | broadband |
| Multi-zone[11] | 4 | source power dependent | zone length | intensity modulated, broadband |
| Multi-zone[12] | N* | N x 500 m | up to 500m | broadband |
| Multi-zone[13] | 2** | 4 times zone length | zone length | 980 nm pump laser |
| The proposed | 2 | up to 16 times zone length | zone length | 1480 nm pump laser |

*N is equal to the number of defended zones if these zones are cascaded in a line pattern. Different wavelengths are allocated for the protected zones.
**Only 4 zones cab be protected. The fiber used is not single-mode fiber, but erbium-doped fiber.

When the RVL is 3.9 V (bottom trace), the optical signal amplitude fluctuates at below 3.9 V, while for a low RVL (top trace) it would fluctuate mostly at above the low RVL. It can be seen that signal oscillation amplitudes are almost the same. i.e., it is independent of reference voltage levels. However, the average voltage of the detected waveform $V_{avg}$ becomes higher as RVL gets higher, and thus the value of NVA would become smaller. We have measured the values of NVA and Ratio over a whole range of RVL. The trend of NVA shown in Fig. 22 justifies our inference. For a low RVL, NVA could go to 8.12 because of a quite small $V_{avg}$ in this case. On the other hand, the value of Ratio can only vary in a narrower range from 0.312 to 0.205. We have also simulated a bird touching case with a gentle touch on the fiber cable for each RVL varying from 0.1 V to 3.9 V. Note that such a gentle touch could result in a larger signal oscillation amplitude with respect to the nonstriking case, but a smaller signal oscillation amplitude with respect to the slight striking case. Figure 23 shows the NVA and Ratio for the cases of nonstriking, bird touching and slight striking. From the figure, we can see that the previous threshold settings for NVA and Ratio (0.9 and 0.18, respectively) would hold for triggering an alarm precisely as the fiber cable is slightly struck, ruling out false alarms by the simulated gentle touch.

## V. DISCUSSION AND CONCLUSION

We have proposed a new optical fiber system for intrusion detection of multiple perimeter zones for the first time by using only two single mode fibers in a fiber cable for each perimeter zone. In the system, each perimeter zone comprises an active unbalanced Michelson interferometer as an end mirror of a fiber laser cavity. Through the phase offset variation induced by vibration of the fiber cable, such an active unbalanced Michelson interferometer behaves as an optical switch and modifies the power of the light oscillation in the laser cavity. One core of the fiber cable is used as an arm of the Michelson interferometer, and the other core is for delivering the pump light down to the individual fiber laser cavities and also for signal light transmission. Usage of the two-core fiber cable can reduce the cost of the PID system implementation, making the proposed system competitive in the field of multi-zone PID. Meanwhile, the outdoor test for the proposed system demonstrates the feasibility of such a multi-zone PID system having not only the advantage of least number of single mode fibers required in the fiber cable but the possibility of achieving precise alarms.

Because the signal power would only be delivered back into the corresponding photodetector without any possibility of entering a different FLC, there is no cross interference between any two perimeter zones. Physically, a signal light (i.e., laser light) from any FLC except the one for perimeter zone 1 would allocate 10 % of its power to the output end of the preceding FC2 that is marked by x (see Fig.1), and this power would not go to the preceding FLC to cause interference for sure. Also, each signal light would follow the one way down to the detection site, and thus would not interfere with the signal lights for subsequent perimeter zones. That is, the laser power of an FLC would not deplete the gain of any other FLC that is provided by the pumped EDF. The outdoor test has confirmed this. Also, we have proved that the false alarm rate could be zero for nonintrusion cases. One thing worth noting is that only one laser needs to be used, and that is for pumping the erbium-doped fibers placed in the remote fiber laser cavities. The rated optical power of the laser determines how many perimeter zones can be put into security. In the case of 20 mW pump power required for each fiber laser cavity, we need at least 320 mW pump power to implement a 16 perimeter zone system. However, we have tested that the required pump power for each perimeter zone can be as large as 10 mW, in which case, only 160 mW pump power in total is required for supporting a 16 perimeter zone security, excluding the fiber transmission loss and the splicing loss between optical components.

Table I below makes a comparison of various intrusion detection techniques, including those techniques mentioned in this paper and the proposed one, addressing the number of fibers used, length of protected area, spatial resolution and the type of light source used. All of the techniques use single-mode fibers for sensors, except the system of [13], which requires erbium-doped fibers to be used for the whole protected area. We can see from the table that the proposed work presents a unique technique for multi-zone systems that use single-mode fibers as sensors, and that this proposed work uses only two fibers in a fiber cable.

Between the zones is a repeater box, which contains fiber couplers, erbium-doped fibers and a bandpass filter in addition to a very short sensing fiber for two neighboring zones. A vibration of the fiber cable at one zone but near the repeater box may influence the short sensing fiber of its neighboring zone, thus causing an instability or crosstalk problem for the neighboring zone. However, we believe this induced vibration

is not big enough to cause a false alarm for the neighboring zone. Two reasons for this are: (1) every repeater box is so tightly fixed somewhere that little vibration can occur. (2) even the repeater box is vibrated, the induced signal oscillation will not be strong enough to cause a false alarm because the sensing fiber for the neighboring zone in the repeater box is short that not much phase change can be induced, and furthermore this short section of fiber in the box would not vibrate ideally speaking since it firmly attaches to the interior surface of the box.

## REFERENCES


[1] M. C. Maki and J. K. Weese, "Fiber optic fence sensor developments," in *Proc. IEEE 37th Annu. Int. Carnahan Conf. Secur. Technol.*, Oct. 2003, pp. 17–22.

[2] A. Yousefi, A. A. Dibazar, and T. Berger, "Intelligent fence intrusion detection system: Detection of intentional fence breaching and recognition of fence climbing," in *Proc. IEEE Int. Conf. Technol. Homeland Secur.*, Boston, MA, USA, May 2008, pp. 620–625.

[3] G. Allwood, G. Wild, and S. Hinckley, "Optical fiber sensors in physical intrusion detection systems: A review," *IEEE Sensors J.*, vol. 16, no. 14, pp. 5497–5509, Jul. 15, 2016.

[4] J. C. Juarez, E. W. Maier, K. N. Choi, and H. F. Taylor, "Distributed fiber-optic intrusion sensor system," *J. Lightw. Technol.*, vol. 23, no. 6, pp. 2081–2087, Jun. 2005.

[5] H. Wang, Q. Sun, X. Li, J. Wo, P. P. Shum, and D. Liu, "Improved location algorithm for multiple intrusions in distributed sagnac fiber sensing system," *Opt. Express*, vol. 22, no. 7, pp. 7587–7597, 2014.

[6] F. Peng, H. Wu, X.-H. Jia, Y.-J. Rao, Z.-N. Wang, and Z.-P. Peng, "Ultra-long high-sensitivity Ø-OTDR for high spatial resolution intrusion detection of pipelines," *Opt. Express*, vol. 22, no. 11, pp. 13804–13810, 2014.

[7] Y. Lu, T. Zhu, L. Chen, and X. Bao, "Distributed vibration sensor based on coherent detection of phase-OTDR," *J. Lightw. Technol.*, vol. 28, no. 22, pp. 3243–3249, Nov. 15, 2010.

[8] D.-P. Zhou, Z. Qin, W. Li, L. Chen, and X. Bao, "Distributed vibration sensing with time-resolved optical frequency-domain reflectometry," *Opt. Express*, vol. 20, no. 12, pp. 13138–13145, 2012.

[9] B. Dong, J. Hao, and V. Paulose, "Armored-cable-based FBG security fence for perimeter intrusion detection with higher performance," *Sens. Actuators A Phys.*, vol. 180, pp. 15–18, Jun. 2012.

[10] P. A. Townley-Smith, S. Hellman, J. Kondis, and E. R. Ranalli, "Perimeter detection using fiber optic sensors," U.S. Patent 7 488 929 B2, Oct. 2, 2009.

[11] A. D. Meyer, "Sensor array for perimeter defense," U.S. Patent 7 526 147 B2, Apr. 28, 2009.

[12] X. Li, Q. Sun, J. Wo, M. Zhang, and D. Liu, "Hybrid TDM/WDM-based fiber-optic sensor network for perimeter intrusion detection," *J. Lightw. Technol.*, vol. 30, no. 8, pp. 1113–1120, Apr. 15, 2012.

[13] S.-L. Woon, K.-M. Kwan, W.-Y. Chong, H.-S. Lin, and C.-H. Pua, "Cascaded acoustic wave sensors based on erbium-doped fiber laser dynamics for intrusion zone identification," *IEEE Sensors J.*, vol. 17, no. 6, pp. 1893–1897, Mar. 2017.

[14] S. S. Mahmoud and J. Katsifolis, "Robust event classification for a fiber optic perimeter intrusion detection system using level crossing features and artificial neural networks," *Proc. SPIE*, vol. 7677, Apr. 2010, Art. no. 767708.

[15] S. S. Mahmoud, Y. Visagathilagar, and J. Katsifolis, "Real-time distributed fiber optic sensor for security systems: Performance, event classification and nuisance mitigation," *Photon. Sensors*, vol. 2, no. 3, pp. 225–236, Sep. 2012.

[16] K.-S. Lin, K.-H. Yeh, Y.-J. Chiang, and L. Wang, "Fiber-optic perimeter intrusion detection by employing a fiber laser cavity in each defensed zone," *IEEE Sensors J.*, vol. 18, no. 20, pp. 8352–8360, Oct. 15, 2018.

[17] J. Zhang *et al.*, "Optical fiber interferometer arrangement method of region anti-intrusion system based on optical fiber interferometer," China Patent 101 901 532 A, 2010. [Online]. Available: http://epub.sipo.gov.cn/

[18] R. Kashyap and B. Nayar, "An all single-mode fiber michelson interferometer sensor," *J. Lightw. Technol.*, vol. 1, no. 4, pp. 619–624, Dec. 1983.



**Hsin Hsieh** received the B.S. degree from the Department of Optics and Photonics, National Central University, Taiwan, in 2015, and the M.S. degree from the Institute of Photonics Technologies, National Tsing Hua University, Hsinchu, Taiwan, in 2018. He is currently a Process Integration Engineer with Vanguard International Semiconductor Corporation, Hsinchu.

**Kai-Shuo Hsu** received the B.S. degree from the Department of Electrical and Control Engineering, National Chiao Tung University, Hsinchu, Taiwan, in 2007, and the M.S. degree from the Department of Electrical Engineering, National Tsing Hua University, Hsinchu, in 2018. He is currently a Senior Firmware Engineer with Sunplus Technology Co., Ltd.

**Tai-Lang Jong** received the B.S. and M.S. degrees from the Department of Electrical Engineering, National Tsing Hua University, Hsinchu, Taiwan, in 1980 and 1982, respectively, and the Ph.D. degree in electrical engineering from Texas Tech University, TX, USA, in 1990. He is currently an Associate Professor with National Tsing Hua University. His research interests include signal processing, biomedical signal processing, neural networks, intelligent systems, and power engineering.

**Likarn Wang** received the B.S. and M.S. degrees in electrical engineering from National Tsing Hua University, Hsinchu, Taiwan, in 1981 and 1983, respectively, and the Ph.D. degree in electrical engineering from Pennsylvania State University, USA, in 1989. He joined the Department of Electrical Engineering, National Tsing Hua University, in 1990, and the Institute of Photonics Technologies, National Tsing Hua University, in 2003, where he is currently a Professor. His research interests include optical fiber sensors and solar cells.